Study of lowlying electronic states of ozone by anion photoelectron spectroscopy of O−3

Don W. Arnold, Cangshan Xu, Eun H. Kim, and Daniel M. Neumark

Citation: J. Chem. Phys. **101**, 912 (1994); doi: 10.1063/1.467745
View online: http://dx.doi.org/10.1063/1.467745
View Table of Contents: http://jcp.aip.org/resource/1/JCPSA6/v101/i2
Published by the American Institute of Physics.

Study of low-lying electronic states of ozone by anion photoelectron spectroscopy of O_3^-

Don W. Arnold, Cangshan Xu, Eun H. Kim, and Daniel M. Neumark[a)]
Department of Chemistry, University of California, Berkeley, California 94720 and Chemical Sciences Division, Lawrence Berkeley Laboratory, Berkeley, California 94720

(Received 27 January 1994; accepted 28 March 1994)

The low-lying electronic states of ozone are studied using anion photoelectron spectroscopy of O_3^-. The spectra show photodetachment transitions from O_3^- to the $\tilde{X}\ ^1A_1$ ground state and to the five lowest lying electronic states of the ozone molecule, namely the $^3A_2$, $^3B_2$, $^1A_2$, $^3B_1$, and $^1B_1$ states. The geometry of the ozonide anion determined from a Franck–Condon analysis of the $O_3\ X\ ^1A_1$ ground state spectrum agrees reasonably well with previous work. The excited state spectra are dominated by bending vibrational progressions which, for some states, extend well above the dissociation asymptote without noticeable lifetime broadening effects. Preliminary assignments are based upon photoelectron angular distributions and comparison with *ab initio* calculations. None of the excited states observed lies below the ground state dissociation limit of O_3 as suggested by previous experimental and theoretical results.

I. INTRODUCTION

As the stratospheric O_3 concentration decreases, so does the protection it offers from harmful ultraviolet radiation. Annual polar ozone depletion has been well documented, particularly in the southern hemisphere.[1] As the polar depletion worsens annually, regions of lower latitude are increasingly affected, in both the southern and northern hemispheres, resulting in a growing public awareness and concern.[2,3] The grave impact which an unchecked ozone depletion will have on the Earth's biological systems has provided the impetus for the present global research effort directed towards determining the causes and effects of ozone depletion. Of the many chemical reactions involved in ozone depletion, the most attention has been given to O_3 destruction cycles catalyzed by the chemical by-products which result from photolysis of man-made chlorofluorocarbons (CFCs) and nitrogen oxides.[4]

In order to understand the underlying chemistry and physics of ozone depletion, a wide range of laboratory experimental studies and high level theoretical calculations have been directed toward the characterization of the O_3 dissociation dynamics and electronic structure. While the electronic spectrum of ozone has been studied extensively, a full characterization is far from complete. The diradical character of ozone leads to the existence of several low-lying excited states, the orbital occupations of which are given in Table I. The $^1B_2 \leftarrow \tilde{X}\ ^1A_1$ transition is responsible for the intense Hartley band centered at 39 000 cm^{-1} (~5 eV). *Ab initio* theory predicts that the other five excited states of ozone listed in Table I lie less than 3 eV (~24 000 cm^{-1}) above the O_3 ($\tilde{X}\ ^1A_1$) state and that the lowest of these lie near the dissociation threshold of the ground state ($D_0 = 1.05$ eV; $D_e = 1.13$ eV).[5–8] Transitions from the ground state to most of these excited states are nominally dipole forbidden, complicating their study by absorption spectroscopy. While these electronic states are not directly involved in absorption of ultraviolet photons, they could play a significant role in ozone recombination kinetics. As a result, atmospheric ozone models and detection methods may be significantly influenced by the properties of these states. This paper describes experiments performed in our laboratory in which we employ anion photoelectron spectroscopy of O_3^- to detect and better characterize the low-lying electronic states of ozone.

The complexity of the O_3 electronic structure below 3 eV is readily apparent from the ozone absorption spectrum. Chappuis[9] and Wulf[10] observed diffuse absorption bands in the visible and near-infrared, respectively, several decades ago, but made no electronic state assignments to the data. The weak, diffuse bands which were observed lie between 9000 and 22 000 cm^{-1}, with a spectral maximum at 16 600 cm^{-1}. Considering the low-lying O_3 electronic states (Table I), only the $^1B_1 \leftarrow \tilde{X}\ ^1A_1$ transition is symmetry allowed from the ground state, while the $^1A_2 \leftarrow \tilde{X}\ ^1A_1$ transition is vibronically allowed via the ν_3 antisymmetric stretch. The remaining three electronic states are triplet states whose absorption transitions from the ground state are spin forbidden. The observation of two absorption bands in this region implies some form of coupling to enable absorption to at least one "dark" electronic state.

The congested electronic structure of O_3 has lead to several contradictory interpretations of the absorption data. Based upon early *ab initio* calculations, the Chappuis and Wulf bands were assigned to the $^1B_1 \leftarrow \tilde{X}\ ^1A_1$ and the $^1A_2 \leftarrow \tilde{X}\ ^1A_1$ transitions, respectively.[11,12] These assignments, however, were insufficient to explain fully the diffuse nature of the Chappuis band or the dissociation dynamics observed by Valentini and co-workers.[13] Vaida *et al.*[14] assigned the Chappuis band to overlapping transitions to the $^1A_2$ state and an unidentified triplet state. This assignment, based on the weakness of the transition ($f \sim 3.2 \times 10^{-5}$) and the enhancement of the Chappuis band relative to the Hartley band in condensed phase absorption,[15] is also questionable as it left no apparent absorption feature to account for the allowed $^1B_1 \leftarrow \tilde{X}\ ^1A_1$ transition.

[a)]NSF Presidential Young Investigator, and Camille and Henry Dreyfus Teacher–Scholar.

 0021-9606/94/101(2)/912/11/$6.00

TABLE I. Single reference configuration of O_3 and O_3^- electronic states.

Electronic state	Configuration
$O_3\ \tilde{X}\ ^1A_1$	$\cdots 1b_1^2 6a_1^2 4b_2^2 1a_2^2 2b_1^0$
$^3B_2/^1B_2$	$\cdots 1b_1^2 6a_1^2 4b_2^2 1a_2^1 2b_1^1$
$^3A_2/^1A_2$	$\cdots 1b_1^2 6a_1^2 4b_2^1 1a_2^2 2b_1^1$
$^3B_1/^1B_1$	$\cdots 1b_1^2 6a_1^1 4b_2^2 1a_2^2 2b_1^1$
$O_3^-\ \tilde{X}\ ^2B_1$	$\cdots 1b_1^2 6a_1^2 4b_2^2 1a_2^2 2b_1^1$

A recent set of experimental and theoretical studies has provided further insight into the assignment of O_3 absorption spectrum. Anderson and co-workers[16] recently utilized isotopic substitution to determine the origins of both the Chappuis and Wulf bands, and have observed rotational structure in the first vibronic transitions of the Wulf band. Theoretical efforts by Braunstein *et al.*[6] and Banichevich *et al.*[8] indicate that the Chappuis band results from the significant interaction between the $^1B_1$ and $^1A_2$ states. This analysis implies that the lower-lying Wulf band is due to transitions to one or more triplet states. Of these, the most likely candidate is considered to be the $^3A_2 \leftarrow \tilde{X}\ ^1A_1$ transition which becomes allowed through a spin–orbit coupling to the $^1B_2$ state ($T_e = 30\,000$ cm^{-1}).[6,16]

Several techniques other than photoabsorption have been used to study O_3 in the visible and near IR regions, some of which have lead researchers to conclude that bound excited states exist below the ground state dissociation limit.[17] Kinetics measurements find a discrepancy for the

$$O(^3P) + O_2(\tilde{X}\ ^3\Sigma_g^-) \xrightarrow{k_{\text{recomb}}} O_3(\tilde{X}\ ^1A_1)$$

recombination rate depending upon whether the rate is determined by measuring the disappearance of $O(^3P)$ ($k_{\text{recomb}} = 6\times10^{-34}$ $cm^6\ s^{-1}$)[18] or the appearance of O_3 ($X\ ^1A_1$) ($k_{\text{recomb}} = 3\times10^{-34}$ $cm^6\ s^{-1}$).[19] Bair and co-workers[20] attribute this discrepancy to the efficient formation (~60%) of a bound excited electronic state. Two sets of emission measurements have been attributed to low-lying electronic states. Von Rosenberg and Trainor[21] discuss the possible assignment of an observed emission peak at 6.6 μm to the $^3B_2 \rightarrow {}^1A_1$ transition, corresponding to an excitation energy of ~1450 cm^{-1}. Shi and Barker[22] postulate that a 1.9 μm emission (0.652 eV, 5263 cm^{-1}) originates from an unidentified excited triplet electronic state of O_3. McGrath *et al.*[23] observe a transient absorption feature with a maximum at 320 nm after primary excitation of O_3 in the 540–650 nm region (Chappuis band). They assign the intermediate as the $O_3(^1A_2)$ state. Swanson and Celotta[24] studied O_3 using electron energy loss spectroscopy (EELS) and observed signal in their data which they attribute to low-lying triplet states. From the analysis of their data, they extrapolated the existence of energy levels for the $^3B_2$ state which are bound with respect to dissociation. Their data are particularly relevant to the present results because the same O_3 electronic states can be observed using EELS and anion photoelectron spectroscopy. However, anion photoelectron spectroscopy has the distinct advantages of mass selectivity and higher spectral resolution. Although this abundance of research has been performed on the visible/near IR region of the O_3 spectrum, no complete state assignment exists and some uncertainty remains concerning whether there are bound excited electronic states which should be considered in atmospheric ozone models.

In this paper, photoelectron spectroscopy of O_3^- is used to provide a more complete picture of the O_3 electronic and vibrational structure. Previously, Novick *et al.*[25] measured the photoelectron spectrum of O_3^- at photodetachment photon energies of 2.540 and 3.407 eV; at these energies, only the O_3 ground state is accessible. The present work explores the properties of several O_3 excited electronic states by using higher photon energies (4.657 and 5.822 eV) and higher resolution electron detection. As demonstrated previously,[26–28] anion photoelectron spectroscopy is complementary to absorption techniques because one is often able to observe optically "dark" states. Considering the single determinant orbital occupation of O_3^- in its $\tilde{X}$ ($^2B_1$) ground state, a one-electron photodetachment of the ozonide anion can yield the O_3 ground state and the six excited states in Table I. Based upon excitation energies predicted by *ab initio* calculations[5–8] and the electron affinity of O_3 determined by Novick *et al.*,[25] all but one of these states, the $^1B_2$ state, should be energetically accessible at 4.657 eV. Photodetachment transitions from O_3^- to all the other five excited states of O_3 do appear in our anion photoelectron spectra. We also obtain the geometry of the O_3^- anion by analyzing the transition to the O_3 ground state, and this is compared to previous results.

II. EXPERIMENT

The apparatus employed in these experiments is a dual time-of-flight anion photoelectron spectrometer. While details of the apparatus have been given elsewhere,[29] a general overview with specifics relevant to the present results will be provided here. In the experiment, anions are generated at the intersection of a pulsed molecular beam and a 1 keV electron beam focused near the orifice of the piezoelectric molecular beam valve[30] operated at 20 Hz. As the molecular beam expansion proceeds, the anions relax vibrationally and rotationally by collisions with the carrier gas. The cooled anions are extracted perpendicularly and injected into a Wiley–McLaren type time-of-flight mass spectrometer.[31] The mass-selected O_3^- ions are selectively photodetached by a properly timed 8 ns light pulse from a Nd:YAG laser. Electron kinetic energies (eKEs) are determined from field-free time-of-flight measurements made on photodetached electrons reaching microchannel plates located at the end of a one meter flight tube. The linearly polarized laser beam can be rotated with respect to the direction of electron collection to study photoelectron angular distributions. This is a very important feature of the experiment which aids the data analysis. When studying the photoelectron angular distributions, the laser polarization is alternated between the desired polarizations in data collection increments of ~40 000 laser shots. The final data result from a summation of those spectra obtained using the same polarization. This procedure ensures that differences in the spectra do not result from a long-term drift of experimental conditions. The resolution of the photoelectron

spectrometer is 7 meV at 0.65 eV and degrades as $(eKE)^{3/2}$ at higher energies. The spectra presented are averaged for approximately 400 000 laser shots each.

Generation of ozonide anions was accomplished by two "synthetic" routes. Initially, O_2 was expanded through the molecular beam valve, at a backing pressure of 4 bar. O^- anions, formed at the molecular beam/electron beam intersection, react with O_2 to form O_3^-,

$$O^- + O_2 \xrightarrow{M} O_3^- . \quad (1)$$

The third body, $M = O_2$, carries away excess energy deposited in the O_3^- internal degrees of freedom upon anion formation ($D_0(O_2-O^-) \sim 1.7$ eV). The resulting photoelectron spectra, not shown, indicate that this ion formation mechanism leads to significant excitation of the O_3^- ν_3 antisymmetric stretch. "Hot bands" resulting from the detachment of vibrationally excited O_3^- anions led to spectral congestion, necessitating the use of second method of ozonide synthesis which produced colder anions. An ozone gas mixture (~0.2% O_3/10% He/~90% Ne) is made by passing the He/Ne mixture over O_3 adsorbed onto silica gel at −78 °C. Ozonide anions are generated by expanding this gas mixture, at a pressure of 1.5 bar, through molecular beam valve, as above. In this case, the O_3^- is most likely produced by electron attachment processes. Ions generated in this way are more efficiently cooled (see Sec. IV A) leading to a less congested spectrum. The data presented here were obtained using the second method of O_3^- preparation.

At the ion densities necessary to obtain sufficient photoelectron signal for O_3^-, the energies of the photodetached electrons are affected by a Coulombic repulsion between the detached electron and the remaining packet of O_3^- ions which are not photodetached. Compensation for this "space-charge" effect is made by first measuring the magnitude of the "space-charge shift" for calibration ions (i.e., O_2^-, Cl^-, Br^-, and I^-) at the same ion densities that were used for O_3^- data collection. The O_3^- data is then corrected by this amount (~5 meV). In addition to the overall shift of the spectrum to higher eKE, there is also a slight broadening of the spectral features (~3 meV). The photoelectron spectra obtained using different photon energies provide information about different regions of the ozone electronic structure as a result of the $(eKE)^{3/2}$ dependence of the experimental resolution. The data sets described below were collected using three different photodetachment energies, two of which are the fourth (266 nm, 4.657 eV; 16 mJ/pulse) and fifth (213 nm; 5.822 eV; 5 mJ/pulse) harmonics of the Nd:YAG laser. The other wavelength (416 nm; 2.977 eV; 5 mJ/pulse) is the first Stokes Raman line generated by focusing the third harmonic of the Nd:YAG laser (355 nm; 3.549 eV; 50 mJ/pulse) into a high pressure (~20 bar) H_2 cell.

III. RESULTS

The photoelectron spectrum of O_3^- measured with a photodetachment energy ($h\nu$) of 2.977 eV is shown in Figure 1(a). Only transitions to the O_3 ($\tilde{X}\ ^1A_1$) ground state are energetically accessible at this photon energy. In general, for a transition to an O_3 electronic state with term value T_0, the eKE is related to the internal energy of the neutral by

$$eKE = h\nu - EA - T_0 - E_v^0 + E_v^- . \quad (2)$$

Here, EA is the electron affinity of O_3, and E_v^0 and E_v^- are the vibrational energies above the zero point of the neutral and anion, respectively. According to Eq. (2), peaks at higher eKE correspond to lower internal energy states of the neutral molecule. The spectrum shown in Fig. 1(a) consists of vibrational progressions in the totally symmetric ν_1 and ν_2 modes of the O_3 ($\tilde{X}\ ^1A_1$) ground state, the origin of which is labeled "*A*" at eKE=0.874 eV. Peak "*a*" is a "hot band" resulting from detachment of vibrationally excited O_3^- anions with $\nu_1 = 1$. Peak positions and assignments are summarized in Table II. Since the geometric parameters and vibrational frequencies of the O_3 ground state have been accurately deter-

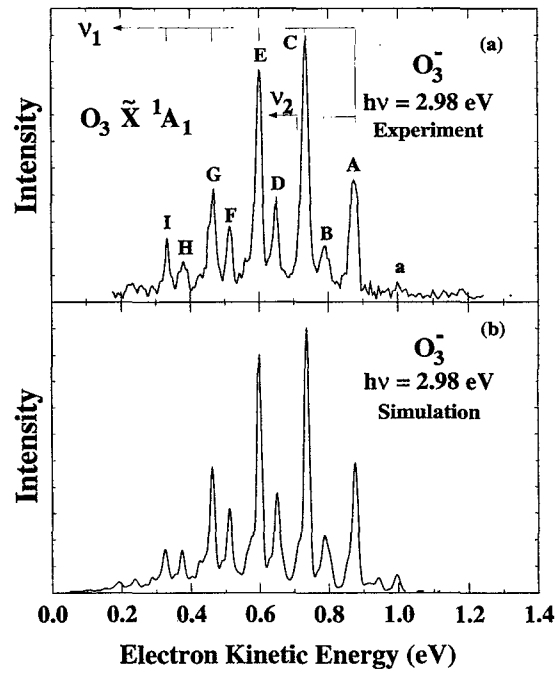

FIG. 1. (a) Photoelectron spectrum of O_3^- measured using a photodetachment energy of 2.977 eV and (b) Franck–Condon simulation of data. See text for details.

TABLE II. Peak positions and assignments[a] for the 2.977 eV O_3^- spectrum.

Peak	eKE (eV)	Assignment
a	1.000	$1_1^0 2_0^0$
A	0.874	0–0
B	0.789	$1_0^0 2_0^1$
C	0.737	$1_0^1 2_0^0$
D	0.649	$1_0^1 2_0^1$
E	0.598	$1_0^2 2_0^0$
F	0.511	$1_0^2 2_0^1$
G	0.462	$1_0^3 2_0^0$
H	0.374	$1_0^3 2_0^1$
I	0.326	$1_0^4 2_0^0$

[a]Assignment notation: $(\nu_1)_{v''}^{v'}(\nu_2)_{v''}^{v'}$.

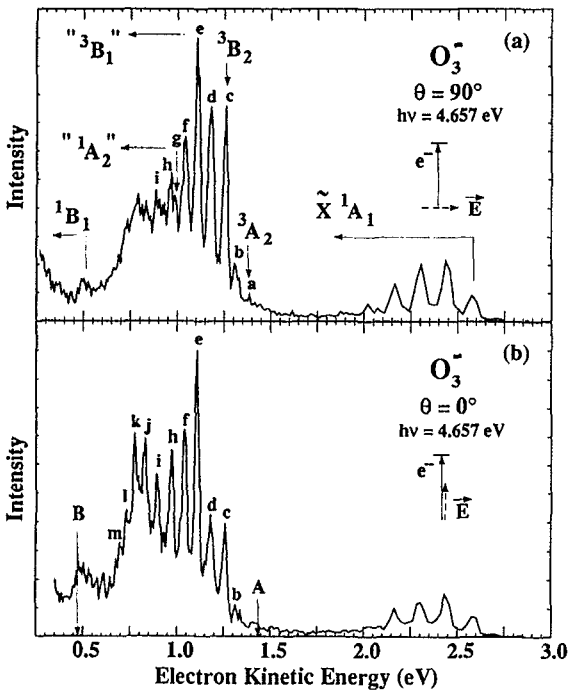

FIG. 2. Photoelectron spectra of O_3^- measured using a photodetachment energy of 4.657 eV at laser polarization angles θ=90° (a) and 0° (b). The laser polarization angle, θ, is the angle between the laser $\vec{E}$ vector and the direction of electron detection. State assignments in Fig. 2(a) are discussed in Sec. IV B 1. In Fig. 2(b), labels "*A*" and "*B*" indicate the dissociation asymptotes for the $O(^3P)+O_2(X\ ^3\Sigma_g^-)$ and the $O(^3P)+O_2(a\ ^1\Delta_g)$ dissociation channels, respectively.

mined, this spectrum can be used in conjunction with a Franck–Condon analysis to determine the geometry of the ozonide anion (see Sec. IV A).

Figures 2(a) and 2(b) show O_3^- spectra collected at a photon energy of 4.657 eV, and laser polarization angles of θ=90° and 0°, respectively. The transitions to the O_3 ($\tilde{X}\ ^1A_1$) ground state occur at eKE>2.0 eV; the peaks are broadened, relative to the corresponding features in Fig. 1(a), due to the higher energy of the detected electrons. In Fig. 2(a) a long progression begins at 1.378 eV, peak "a," with an average peak spacing of 555±50 cm^{-1} evolving into a very congested feature beginning at ~0.9 eV. Peak positions are given in Table III. Based upon agreement with the maximum in the Chappuis band absorption,[16(b)] the peak at ~0.5 eV is assigned as the transition to the $^1B_1$ state [T_e=2.046 eV (Ref. 16)]. By default, the long progression must represent transitions to one or more of the lower lying "optically forbidden" states of O_3. In contrast to O_3 absorption experiments, O_3^- photodetachment transitions to these states are vibrationally resolved and are more intense than the transition to the $^1B_1$ state.

While the peaks in the long progression of Figure 2(a) are approximately evenly spaced, there are several indications that this is not simply a progression in a single vibrational mode of an O_3 excited state. For example, Table III shows that there are significant variations in the peak spacings and widths. The intensity distribution is quite irregular,

TABLE III. Peak positions for the 4.657 eV O_3^- spectrum.

Peak	eKE (eV)	Width[a] (FWHM; eV)
a	1.378	...
b	1.304	0.037
c	1.257	0.032
d	1.177	0.047
e	1.105	0.032
f	1.039	0.040
g	0.984	~0.025[b]
h	0.967	~0.025[b]
i	0.890	c
j	0.827	c
k	0.772	c
l	0.726	c
m	0.694	c

[a]Peak widths determined from θ=90° data.
[b]Estimate based upon deconvolution into two Gaussian peaks with FWHM =0.025 eV.
[c]Estimated FWHM <0.025 eV on top of background structure.

and does not resemble the typical Franck–Condon profile for a single vibrational mode. Rather, it appears that this progression is actually composed of a series of overlapping transitions. To characterize it further, it is useful to examine the dependence of the features in the photoelectron spectrum on the laser polarization direction.

The photoelectron angular distribution resulting from O_3^- photodetachment to a particular O_3 electronic state is given by Eq. (3),[32] where σ_{tot}(eKE) is the total cross section for photodetachment, β(eKE) is the asymmetry parameter ($-1\leq\beta\leq 2$), and θ is the angle between the laser polarization and the direction of electron collection:

$$\frac{d\sigma}{d\Omega}=\frac{\sigma_{tot}(\text{eKE})}{4\pi}\cdot\left(1+\frac{\beta(\text{eKE})}{2}\cdot(3\cos^2\theta-1)\right). \quad (3)$$

The asymmetry parameter, β, is not expected to change rapidly for transitions to different vibrational levels of the same neutral electronic state, but it can be very different for transitions to different electronic states. Hence, a marked variation of peak intensities with laser polarization provides a means of determining the presence of overlapping transitions to multiple electronic states.

There are significant differences between the spectra in Figs. 2(a) and 2(b). Peaks "*c*" and "*d*" are considerably less intense in the θ=0° spectrum, and the intensity discontinuity between peaks "*d*" and "*e*" is much more noticeable in Fig. 2(b). At lower eKE, peaks "*h*" and "*i*" are more intense in the θ=0° spectrum, and several new peaks ("*j*"–"*m*") are apparent on top of what was only a broad unstructured feature in the θ=90° spectrum. Additional polarization studies are shown in Figs. 3(a) and 3(b). These are O_3^- photoelectron spectra collected at θ=90° and θ=0°, respectively, using a 5.822 eV photodetachment photon energy. The spectral features, broadened due to their positions at higher eKEs, exhibit a polarization dependence similar to that observed in the 4.657 eV data. This confirms that the polarization effects seen in Fig. 2 are not due to the energy dependence of the asymmetry parameter, but rather to the existence of overlapping transitions to multiple electronic states. Detachment

TABLE IV. Calculated and experimental properties of electronic states of ozone.

State	Theory	r_e (Å)	θ_e (degrees)	ω_1 (cm^{-1})	ω_2 (cm^{-1})[a]	T_e (eV)	Reference
O_3 $^1A_1$	POL–CI	1.299	116	1235.0	707.0	0.0	b
	MCSCF+CI	1.277	116.1	1173.0	737.1	0.0	c
	MRD-CI	1.29	116.0	1105	704	0.0	e
Expt.	···	1.2717	116.7	1135	716	0.0	g
$^3B_2$	POL-CI	1.382	107.9	1112.0	645.0	0.92	b
	MCSCF+CI	1.360	108.3	1176.4	624.6	1.09	d
	MRD-CI	1.34	108.5	1276	600	1.10	e
Expt.	···	···	···	···	580(50)[i]	T_0=1.30	h
$^3A_2$	POL-CI	1.366	99.7	1167.0	535.0	1.35	b
	MCSCF+CI	1.348	101.5	1224.0	552.8	1.34	d
	MRD-CI	1.36	103.6	1288	552	0.86	e
Expt.	···	···	···	···	528(15)	T_0=1.18	f
	···	···	···	···	530(50)[i]	T_0=1.18	h
$^3B_1$	POL-CI	1.347	123.8	915.0	518.0	1.74	b
	MCSCF+CI	1.343	121.3	932.1	520.4	1.78	d
	MRD-CI	1.36	123.5	1083	662	1.27	e
	Expt.	···	···	···	560(50)[i]	T_0=1.45	f
$^1A_2$	POL-CI	1.374	100.7	1160.0	537.0	1.66	b
	MCSCF+CI	1.351	101.5	1182.7	598.2	1.57	c
	MRD-CI	1.34	100.0	1093	675	1.44	e
	Expt.	···	···	···	690(100)[j]	T_0~1.6	h
$^1B_1$	POL-CI	1.370	117.7	965.0	489.0	2.06	b
	MCSCF+CI	1.362	116.2	1004.6	509.4	2.01	c
	MRD-CI	1.35	117.2	1091	476	1.82	e
$^1B_2$	POL-CI	1.405	108.4	···	···	5.54	b
	MRD-CI	1.38	110.1	1235	574	4.34	e

[a]Values in parentheses are estimated experimental uncertainties.
[b]Polarization configuration interaction—Ref. 5(a).
[c]Multireference self-consistent field+configuration interaction—Ref. 6(a).
[d]Multireference self-consistent field+configuration interaction—Ref. 6(b).
[e]Multireference with single and double excitations+configuration interaction—Ref. 7.
[f]Reference 16.
[g]Reference 35.
[h]Present work.
[i]Values are based upon Franck–Condon simulations (not shown) which enable deconvolution of varied peak widths and spacings.
[j]Based upon least-squares analysis of peaks "*h*" through "*m*" giving ω_e=694 cm^{-1} and $x_e\omega_e$=42 cm^{-1}.

transitions to the $^1B_1$ state become more prominent in the 5.822 eV spectrum and exhibit a strong polarization dependence as well. The spectra show no evidence of higher lying electronic states which would appear at lower eKE.

The intensities and polarization dependence of the peaks in Figures 2(a) and 2(b) suggest that the long progression beginning at eKE=1.378 eV consists of transitions to four electronic states of O_3, with origins at peaks "*a*", "*c*", "*e*", and "*h*". These states lie between the O_3 ground state and the $^1B_1$ excited states. The remaining low-lying excited states are the $^3A_2$, $^3B_2$, $^3B_1$, and $^1A_2$ states, and it appears we are observing transitions to all of these. The specific assignment of the features in the photoelectron spectra to these states will be discussed further in Sec. IV B.

IV. ANALYSIS AND DISCUSSION

The data presented in Sec. III provide information about the ground state and the five lowest-lying electronic states of O_3. In Sec. IV A, the analysis of the 2.977 eV O_3^- photoelectron spectrum is discussed. A Franck–Condon analysis of the O_3 ($\tilde{X}$ $^1A_1$) ground state spectrum provides the ozonide geometry. In Sec. IV B, the 4.657 eV spectrum of the ozone excited states is considered and compared with previous experimental and theoretical results (Table IV).

A. 2.977 eV–O_3^-→O_3($\tilde{X}$ $^1A_1$): Determination of the O_3^- geometry

While Novick *et al.*[25] previously obtained photoelectron spectra of O_3^-, the present results are of sufficiently higher resolution to resolve the O_3 ($\tilde{X}$ $^1A_1$) ν_2 bending progression which was not observed in their data. The electron affinity of ozone, determined from the position of the 0–0 peak in the spectrum and Eq. (2), EA(O_3)=2.103±0.004 eV, agrees well with the value previously determined by Novick *et al.*[25] using threshold photodetachment [EA(O_3)=2.1028±0.0025 eV].

The length of the observed vibrational progression provides information about the changes in equilibrium geometry

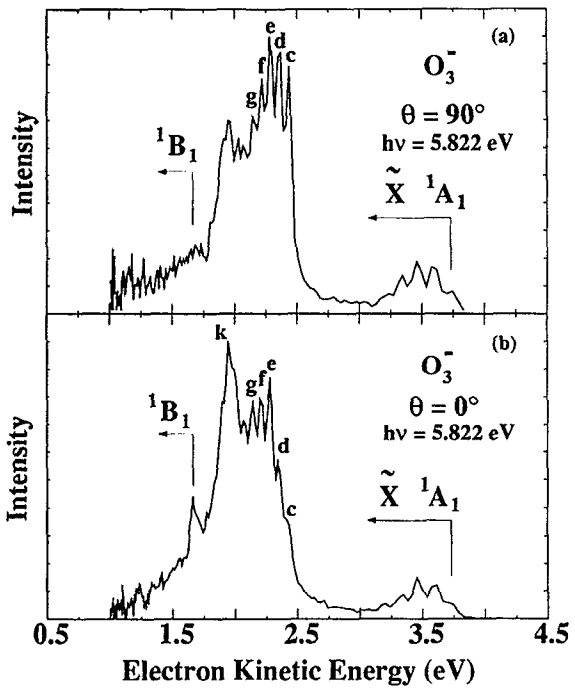

FIG. 3. Photoelectron spectra of O_3^- measured using a photodetachment energy of 5.822 eV at laser polarization angle θ=90° (a) and 0° (b). Peak labels are consistent with those used in Fig. 2.

between O_3^- and O_3. The long symmetric stretch progression indicates that there is a significant difference between the bond lengths of the anion and neutral. The shorter progression in the bending mode shows that the bond angles also differ but not as substantially. To determine the direction of these geometry changes, it is useful to consider the molecular orbital from which the electron is detached to form the O_3 $\tilde{X}\ ^1A_1$ ground state. As indicated in Table I, the HOMO (highest occupied molecular orbital) of the ozonide anion is a b_1 antibonding π orbital. Removal of this electron should lead to a bond length decrease and a bond angle increase, making $r_{O\text{-}O}(O_3)\langle r_{O\text{-}O}(O_3^-)$ and $\theta(O_3)\rangle\theta(O_3^-)$.

Through the use of a Franck–Condon analysis and normal mode calculations, a quantitative determination of the ozonide anion geometry is possible following, for example, the treatment of the NO_2^- photoelectron spectrum of Ervin *et al.*[33] The normal modes, Q_i, are assumed to be separable and parallel (i.e., the form of the normal coordinates in the anion and neutral are the same), in which case the transition intensity, I, for the process

$$O_3^-(v_1'',v_2'',v_3'')\xrightarrow{h\nu}O_3(v_1',v_2',v_3')+e^- \tag{4}$$

is given by[34]

$$I\propto v\cdot|\tau_e|^2\cdot\prod_{i=1}^{3}|\langle\psi_{v_i'}(Q_i)|\psi_{v_i''}(Q_i)\rangle|^2. \tag{5}$$

The Franck–Condon factor, $|\langle\psi_{v_i'}|\psi_{v_i''}\rangle|^2$, is the spatial overlap of the vibrational wave functions for the ith vibrational mode of the anion, $\psi_{v_i''}$, and neutral, $\psi_{v_i'}$. The electronic transition dipole moment, τ_e, is assumed to be constant over the energy range spanned by a vibrational progression for a particular electronic state, and v is the asymptotic velocity of the detached electron.

The Franck–Condon factors (FCFs) are calculated using known structural parameters (r_e=1.2717 Å, θ_e=116.7°), vibrational frequencies and primary anharmonicities (ω_1=1135 cm^{-1}, ω_2=716 cm^{-1}, ω_3=1089 cm^{-1}, x_{11}=4.9 cm^{-1}, x_{22}=1.0 cm^{-1}, x_{33}=10.6 cm^{-1}) of the ozone ground state.[35] The ν_1 and ν_2 modes of O_3 are modeled with Morse potentials derived from these vibrational parameters. Anharmonic effects are most important for the ν_1 symmetric stretch mode, as this is the longest progression in the spectrum. The ν_3 normal coordinate change, ΔQ_3, is constrained to be zero by symmetry, and anharmonicity of this mode is neglected in the simulation shown in Fig. 1. As the gas phase vibrational frequencies and anharmonicities for the anion vibrational modes are not as accurately established, the frequencies are adjusted in the simulation to obtain the best agreement with the data (i.e., peak "*a*" in Fig. 1) and previous observations (see Table V). The O_3^- harmonic frequencies employed in the simulation are ω_1=975 cm^{-1}, ω_2=550 cm^{-1}, and ω_3=880 cm^{-1}. A vibrational temperature of 550 K was assumed in the simulations. At this temperature, most of the anions (~65%) are in their ground vibrational state. As a result, anion anharmonicities have minor effects on the simulations which contribute to the stated uncertainties below. The calculated FCFs are convoluted with the experimental resolution and an additional 4 meV Gaussian peak to account for unresolved rotational contours and "space-charge" broadening effects (see Sec. II).

The simulation in Fig. 1(b) is obtained by varying the ν_1 and ν_2 normal coordinate displacements between the anion and neutral to obtain the best agreement with the experimental spectrum. It is possible to determine the O_3^- geometry, provided we can determine the sign of the normal coordinate displacements. Based on the molecular orbital considerations discussed above, one expects a longer bond length and more acute bond angle in the anion. These expectations are supported by considering effects due to anharmonicity, which break the symmetry of the harmonic oscillator potential. Specifically, the ν_1 anharmonicity leads to a more attractive potential at longer bond lengths. As a result, no acceptable simulation for the spectrum could be calculated if the bond length displacement was in the opposite direction [i.e., when $r_{O\text{-}O}(O_3)>r_{O\text{-}O}(O_3^-)$]. For the ν_2 bending mode, the anion is assumed to have a more acute bond angle than the neutral and a more repulsive wall at smaller bond angles.

Once the normal mode displacements are determined, the geometry changes and hence the O_3^- geometry are determined using an FG-matrix vibrational analysis.[36] In the parallel mode approximation, the same force constants are used in the F matrix for both the anion and neutral; in this case, the O_3 force constants are those determined by Hennig *et al.*[37] The overall analysis yields $r_e(O_3^-)$=1.36±0.02 Å and $\theta_e(O_3^-)$=111.8±2.0°.[38]

Comparison of the ozonide geometry obtained from this analysis with other experiments and theoretical studies finds reasonable agreement in many cases and a slight disagreement in others. Excellent agreement is found with the results

TABLE V. Calculated and experimental properties of the ozonide anion ground state.

O_3^- $\tilde{X}$ $^2B_1$	r_e (Å)	θ_e (degrees)	ω_1 (cm^{-1})	ω_2 (cm^{-1})	ω_3 (cm^{-1})	Reference
Theory	1.385	115.4	976	552	···	a
	1.35	114.5	···	···	···	b
	1.361	115.4	992	572	879	c
Expt.	···	110±5	···	···	800	d
	1.3414±0.03	112.6±2.0	···	···	···	e
	···	···	(a)790±50	(a)419±20	···	f
			(b)928±50	(b)403±20		
	···	···	975±10	590±10	···	g
	See text and Ref. 25		982±50	550±50	···	h
	1.36±0.02	111.7±2.0	975±50	550±50	880±50[i]	j

[a]K. A. Peterson, R. C. Mayrhofer, and R. C. Woods, J. Chem. Phys. **93**, 5020 (1990).
[b]W. Koch, G. Frenking, G. Steffen, D. Reinen, M. Jansen, and W. Assenmacher, J. Chem. Phys. **99**, 1271 (1993).
[c]R. González-Luque, M. Merchán, P. Borowski, and B. O. Roos, Theor. Chim. Acta **86**, 467 (1993).
[d]Reference 41.
[e]Reference 39.
[f]J. F. Hiller and M. L. Vestal, J. Chem. Phys **74**, 6096 (1981).
[g]P. C. Cosby, J. T. Moseley, J. R. Peterson, and J. H. Ling, J. Chem. Phys. **69**, 2771 (1978).
[h]Reference 25.
[i]Determined from sequence bands of unpublished spectrum of vibrationally excited O_3^-.
[j]Present work.

of a vibrationally resolved O_3^- photodetachment total cross-section measurement [$EA(O_3)=2.082\pm0.040$ eV; $r(O_3^-)=1.3414\pm0.0300$ Å; $\theta(O_3^-)=112.6\pm2.0°$] by Wang *et al.*[39] Matrix isolation spectroscopy results[40] determine $\theta_e(O_3^-)$ bond angles between 105° and 119°. Since alkali counterions may distort the geometry of the anion, O_3^- has been studied in an Ar matrix without counterions[41] to yield $\theta_e(O_3^-)=110\pm5°$. The isoelectronic species, SO_2^-, undergoes a similar geometric rearrangement upon photodetachment ($\Delta r_0=0.09$ Å, $\Delta\theta_0=3.9°$).[42] Our ozonide geometry does not lie on the seam of geometries derived from a Franck–Condon analysis of the photoelectron spectrum obtained by Novick *et al.*[25] This disagreement stems from the effect which the newly resolved bending progression produces in the normal coordinate analysis. Recent *ab initio* calculations predict O_3^- bond lengths in agreement with the present results but predicts a larger bond angle than that determined from the photoelectron spectrum (see Table V). Our geometry changes are close to those obtained by Cederbaum *et al.*[43] in their calculation of the O_3 radiative attachment spectrum.

B. O_3 Excited states

As discussed in Sec. III, the 4.657 eV O_3^- spectrum appears to represent photodetachment transitions to the ground state and the five lowest-lying excited states of the ozone molecule. In this section, these excited state bands will be discussed in more detail. Comparisons will be made with other experimental results and with the predictions of *ab initio* calculations in an effort to assign features of the spectrum to specific O_3 electronic states. In addition, we will consider the exceptional amount of vibrational structure seen in the O_3^- photoelectron spectrum, much of which lies well above the dissociation asymptotes of the electronic states observed.

1. Assignment of the O_3 excited electronic states

The intensity distribution and polarization dependence of the spectral features in Fig. 2 imply that transitions to five excited O_3 states occur in the $h\nu=4.657$ eV photoelectron spectrum. In addition to the $^1B_1$ state at eKE=0.5 eV, excited state origins occur at eKEs of 1.378, 1.257, 1.105, and 0.97 eV (peaks "*a*", "*c*", "*e*", and "*h*," respectively). These correspond to excitation energies (T_0) of 1.18, 1.30, 1.45, and 1.58 eV, respectively. As indicated in the Fig. 2(a), the origin of the Wulf band, as determined by Anderson and co-workers ($T_0=1.18\pm0.01$ eV),[16] is expected to lie at eKE $=1.371$ eV in reasonable agreement with the position of peak "*a*." Anderson and co-workers have recently obtained independent evidence that excited states may exist at excitation energies of 1.29 and 1.45 eV using absorption and isotopic substitution techniques.[44] These energies are in excellent agreement with the positions of peaks "*c*" and "*e*," respectively. No evidence for an excited state with $T_0=1.58$ eV has been found in any absorption spectra as of yet.

The assignment of these features to specific electronic states is complicated by the considerable spectral overlap among the bands. As a first step, it is useful to address only geometric considerations. As discussed in Sec. III A, the geometric differences between the anion and neutral govern the Franck–Condon factors and thus the vibrational profile for each electronic state. Based on the *ab initio* geometries in Tables IV and V, one expects significant bending mode excitation upon photodetachment of the ozonide anion for the $^3A_2$, $^3B_1$, and $^1A_2$ states and very little vibrational excitation for the $^3B_2$ and $^1B_1$ states. Since the bond lengths of the excited states are approximately equal to that determined for the anion, very little excitation of the symmetric stretch is expected for any of the excited states observed. As a general rule, excitation of nontotally symmetric vibrational modes (ν_3) is not expected unless a large frequency difference exists

between the anion and the neutral in that mode.

Ab initio predictions of the excited state energies (see Table IV) are also helpful in assigning the spectra. High level *ab initio* calculations have predicted various orderings of the electronic states, depending upon the level of theory employed.[5–8] While all of the states are fairly low lying, the $^3A_2$ and $^3B_2$ states are usually found to be the lowest excited states and fluctuate above or below the dissociation asymptote of O_3 depending upon the calculation performed.

Summarizing our expectations based on *ab initio* calculations, the two lowest excited states are the $^3A_2$ state with a long vibrational progression and the $^3B_2$ state with a short progression. However, the energetic ordering of the two states is undetermined. These two states are expected to lie below the $^1A_2$ and the $^3B_1$ states, both of which should have long bending progressions. To agree with the Chappuis band assignment, the $^1A_2$ should be energetically proximal to the $^1B_1$ state.

Turning to the photoelectron spectra in Fig. 2, it appears that peaks "*a*" and "*b*" are the beginning of a long vibrational progression, whereas peaks "*c*" and "*d*" are part of a considerably shorter progression. From the above discussion, we would assign peaks "*a*" and "*c*" to the origins of the $^3A_2$ and $^3B_1$ states, respectively. As a more quantitative comparison between theory and experiment, one can easily generate a simulated photoelectron based upon the output of *ab initio* calculations within the separable normal mode approximation. These simulations require the calculation of geometries and force constant matrices so that the normal coordinate displacements can be calculated. Since configuration interaction (CI) is known to be significant for most of the O_3 electronic states considered, the calculations must include these effects. We have carried out CI calculations with single and double excitations (SCF-CISD) within a standard 6-31G basis set using the GAUSSIAN 92 package.[45] As we are only interested in the totally symmetric modes, the calculation is restricted to geometries with C_{2v} symmetry. While not as extensive as previously published calculations, the geometries and frequencies are in reasonable agreement[46] with the higher level results in Table IV, so the force constants should be sufficiently accurate for our purposes.

For each O_3 excited state, the normal coordinates for the ν_1 and ν_2 modes are obtained by diagonalization of the *ab initio* Cartesian force constant matrix, and the normal coordinate displacements between the anion (using our experimentally determined geometry) and each neutral state are determined within the parallel mode approximation. We then calculate Franck–Condon factors for the two anion→neutral transitions as in Sec. IV A, again assuming an anion vibrational temperature of 550 K.

The resulting simulations for the $^3A_2$ and $^3B_2$ states are shown in Fig. 4(a) and 4(b), respectively. As expected, the bending progression for the transition to the $^3B_2$ state is considerably shorter than that of the $^3A_2$ state. In Fig. 4(c) and 4(d), these simulations are superimposed on the experimental spectra at laser polarization angles θ=0°, and 90°, respectively. Here, the $^3A_2$ state is assigned to the Wulf band beginning at eKE=1.378 eV, peak "*a*", and the $^3B_2$ state to the state beginning at eKE=1.257 eV, peak "*c*." By combining

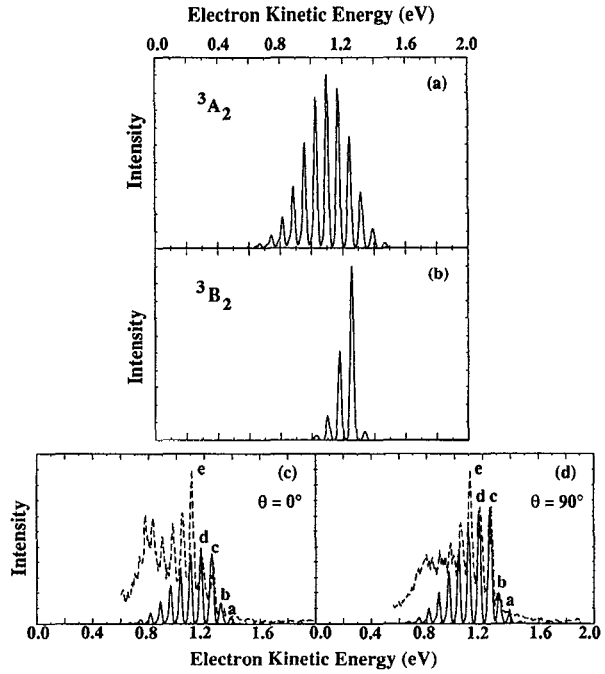

FIG. 4. [(a) and (b)] Franck–Condon calculations for photodetachment to the O_3 $^3A_2$ and $^3B_2$ electronic states using *ab initio* calculated geometries and vibrational frequencies and the experimentally determined O_3^- geometry (See Sec. IV B for details). [(c) and (d)] Simulations (solid lines) are scaled and summed to fit first several peaks in the 4.657 eV experimental spectra (dashed lines) collected at laser polarizations of θ=0° and 90°. Origins of $^3A_2$ and $^3B_2$ states are assumed to be peaks "*a*" and "*c*," respectively. Scaling factors are $(0.42\cdot{}^3A_2+0.3\cdot{}^3B_2)$ in Fig. 4(c) and $(0.53\cdot{}^3A_2+0.53\cdot{}^3B_2)$ in Fig. 4(d).

scaled $^3A_2$ and $^3B_2$ simulations, as indicated in the Figure caption, one can approximately simulate the peak intensities at both laser polarizations for peaks "*a*"-"*d*." This cannot be done if the assignment of the origins is reversed. Beginning at peak "*e*," another state begins to contribute to the spectrum, hence its greater intensity and different polarization dependence. Overall, the simulations support our assignment of the $^3A_2$ and $^3B_2$ states. Our assignment of the $^3A_2$ state is consistent with that of Braunstein *et al.*[6(b)]

The two electronic states which remain unassigned are the $^3B_1$ and the $^1A_2$ states. As mentioned above, long progressions are expected for both the $^1A_2$ and the $^3B_1$ states. However, one of the two remaining states in the spectra, beginning at peak "*e*," has only a medium length ν_2 progression. Thus, the simple considerations of geometry and energy are insufficient to determine a specific assignment of these states. No additional assistance is gained from calculated vibrational frequencies for these states since at each level of theory investigated, both states have similar ν_2 frequencies (Table IV). However, the recent *ab initio* calculation by Banichevich and Peyerimhoff[7] predicts the $^1A_2$ state to lie 0.17 eV above the $^3B_1$ state, suggesting that the origins of the two states should be assigned to peaks "*h*" and "*e*," respectively, with T_0 values of 1.58 and 1.45 eV. This assignment, particularly that of the $^1A_2$ origin, must be considered as tentative, however. While the most consistent assignment

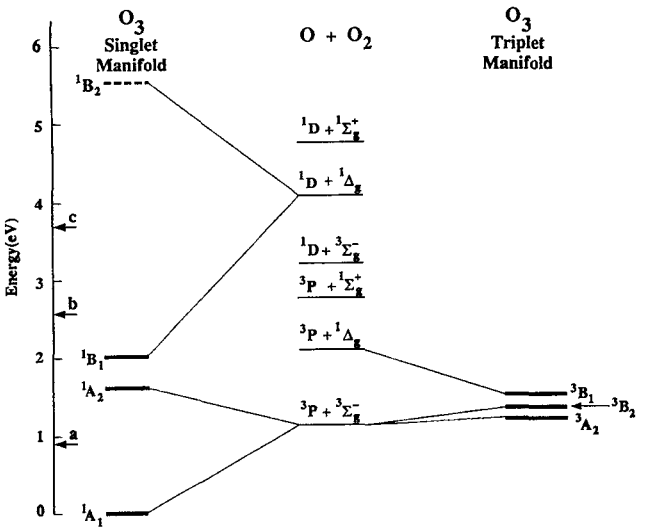

FIG. 5. Correlation diagram for O_3 in C_{2v} symmetry adapted from Hay and Dunning [Ref. 5(c)]. The relative energies of the electronic states have been modified to reflect the preliminary assignments made from the spectra presented. The $^1A_2$ and $^3B_1$ ordering is tentative. The arrows marked "*a*," "*b*," and "*c*" indicate the highest energies accessible using the 2.977, 4.657, and 5.822 eV photodetachment energies, respectively.

of the $^1A_2$ origin is to peak "*h*," it is not definitive due to the spectral congestion in this region.

As mentioned above, the variation of peak widths in the spectrum most likely results from the convolution of nearly overlapping transitions to different electronic states. Deconvolution of the irregular peak widths and spacings through a Franck–Condon analysis (not shown) provides the ν_2 vibrational frequencies for the $^3A_2$, $^3B_2$, and $^3B_1$ electronic states. The values, which differ from the raw spacings of the peak centers, are included in Table IV along with the excitation energies of these states determined from the data.

The one aspect of the spectra not discussed so far is the broad feature around eKE=0.75 eV in Fig. 2(a). This band could result from very rapid dissociation of the higher lying vibrational levels of one the O_3 excited states, most likely the one with its origin at peak "*e*." Alternatively, the width of this feature could be entirely heterogeneous, and due instead to overlapping vibrational transitions from several electronic states. While one might hope to distinguish between these possibilities with laser polarization effects, the polarization dependence of this feature is difficult to determine as it is obscured by peaks "*i*"–"1" in Fig. 2(b).

2. O_3 excited state dissociation dynamics

We next consider in greater detail what the photoelectron spectrum of the O_3 excited states reveals about their energetics and dissociation dynamics. All of the O_3 excited states accessed in the photoelectron spectrum lie above the dissociation threshold to ground state $O(^3P)+O_2(X\ ^3\Sigma_g^-)$ products. Since all of the low-lying excited states of O_3 have been accounted for, this means there are no bound excited electronic states of O_3. This result is relevant to atmospheric chemistry since it rules out the possibility of a bound excited state affecting the $O+O_2$ recombination rate; the discrepancy in this rate measurement discussed in the Introduction must come from another source.

Since all of the excited states have sufficient energy to dissociate, the presence of so much well-resolved vibrational structure in the excited state region of the photoelectron spectrum is of considerable interest. The observation of vibrational structure in transitions to dissociative electronic states in both absorption and photoelectron spectra is well known, and can occur through a variety of mechanisms. The simplest explanation for the current case is suggested by the correlation diagram in Fig. 5, adapted from the work of Hay and Dunning.[5(c)] This shows that the $^3A_2$, $^3B_2$, and $^1A_2$ states correlate to ground state $O(^3P)+O_2(X\ ^3\Sigma_g^-)$ products, whereas the $^3B_1$ and $^1B_1$ states correlate to excited $O(^3P)+O_2(a\ ^1\Delta_g)$ and $O(^1D)+O_2(a\ ^1\Delta_g)$ products, respectively. Thus, both of the latter states lie below their respective asymptotic channels. One can therefore imagine that the structure in the transitions to the $^3B_1$ and $^1B_1$ states arises because they are long-lived states that undergo predissociation. On the other hand, the lower three states lie above the asymptotic channel to which they correlate. Even if these states are purely repulsive along the dissociation coordinate (the Q_3 antisymmetric stretch coordinate in the Franck–Condon region), structure can arise in the spectrum if the dissociating molecule undergoes vibrational motion along the bound symmetric stretch and bend coordinates on the same time scale as dissociation. Such a mechanism has been proposed for structured absorption bands in several small molecules.[47,48]

As an exemplary application of this latter mechanism to the electronic spectroscopy of O_3, Braunstein and Pack[6(b)] have simulated the O_3 $^3A_2 \leftarrow {}^1A_1$ band, which is allowed via spin–orbit coupling between the $^3A_2$ and $^1B_2$ states (the latter is responsible for the very strong Hartley band around 250 nm). Even though the $^3A_2$ potential energy surface was assumed to be repulsive along the Q_3 coordinate, the simulated spectrum shows a resolved bend progression that approximately matches the structure seen in the Wulf band of O_3. However, a very recent reinvestigation of the Wulf band by Anderson and co-workers uncovered resolved rotational structure in the first few vibrational bands.[16] While the above mechanism enables vibrational structure to survive for dissociative states, the presence of this rotational structure suggests the existence of a barrier to dissociation along the Q_3 coordinate. Anderson *et al.* estimate the height of this barrier to be on the order of ~0.1 eV.

A more complex mechanism has been proposed by Braunstein *et al.*[6] and Banichevich *et al.*[8] to explain the diffuse structure observed in the O_3 Chappuis band. Specifically, when O_3 is restricted to C_{2v} symmetry, the $^1B_1$ and $^1A_2$ states intersect near the Franck–Condon region for absorption from the O_3 ground state. However, both states have $^1A''$ symmetry in the C_s point group, so the two states repel each other if there is any displacement along the O_3 antisymmetric stretch coordinate. This results in a conical intersection when the full three dimensional potential energy surfaces for the two states are considered. While the lower 1 $^1A''$ state is repulsive along the Q_3 coordinate, the upper 2 $^1A''$ state (the

"cone" state) can support vibrational levels which are bound along all three coordinates, although they couple to the lower repulsive state via non-adiabatic interactions. Both sets of calculations indicate that the 2 $^1A''$ state is responsible for the partially resolved vibrational structure in the O_3 Chappuis band. A conical intersection between the $^3A_2$ and $^3B_1$ states is also predicted to occur near the Franck–Condon region, but the effect this has on the absorption spectrum has not been considered in detail.

The same mechanisms responsible for structure in the absorption spectrum can be applied to excited state region of the O_3^- photoelectron spectrum. However, it is noteworthy that the photoelectron spectrum is more structured than the absorption spectrum; one might have instead expected the photoelectron spectrum to be more congested because transitions to more electronic states are allowed. Several possible causes for these differences could arise from the different Franck–Condon regions for photodetachment vs. absorption. For example, while photodetachment of O_3^- to the O_3 excited states primarily excites the ν_2 bending mode, the O_3 $^1A_2 \leftarrow {}^1A_1$ transition will excite both the bend and the ν_1 symmetric stretch, further congesting the absorption spectrum. One should also consider the proximity of the Franck–Condon region to the conical intersection between the $^1B_1$ and $^1A_2$ states, which occurs near $\theta = 120°$ over a wide range of O_3 bond lengths. Since the O_3^- bond angle is smaller than that of the neutral (see Sec IV A), the photodetachment Franck–Condon region is farther from the conical intersection than that for absorption. For $r_{O-O} = 1.35$ Å, approximately the bond length of the anion, Braunstein and Pack[6] clearly illustrate that as the bond angle is changed from $\theta \sim 120°$ the potential energy surface along the Q_3 coordinate of the 1 $^1A''$ state becomes less repulsive. The 1 $^1A''$ state flattens along Q_3 due to weaker interaction with the upper 2 $^1A''$ state at the anion geometry. The flatter surface may lead to slower dissociation and a more structured spectrum. Similar effects may also occur in the triplet manifold where the conical intersection occurs at approximately the same bond angle as for the singlet states. The lower energy triplet surfaces are already closer to the dissociation limit so that they must be less repulsive along the dissociation coordinate anyway.

Photodetachment and absorption transitions to the O_3 ($^1A_2$) state differ in another significant respect. In absorption, the $^1A_2 \leftarrow {}^1A_1$ transition is only vibronically allowed via the antisymmetric stretch; thus, this absorption process necessarily includes ν_3 excitation. Along the Q_3 coordinate, the $^1A_2$ potential energy surface has a maximum at $Q_3 = 0$ and slopes downward to $O + O_2$ dissociation products at $|Q_3| > 0$. The effect of this on the dissociation dynamics can best be pictured in the language of wave packets.[47(c)] As Braunstein and Pack[6] point out, the initial $t = 0$ wave packet placed on the $^1A_2$ surface by absorption has a node at the relatively flat $Q_3 = 0$ barrier and the greatest amplitude at a non zero value of Q_3 on the repulsive part of the potential. As a consequence, simulated spectra of the $^1A_2 \leftarrow {}^1A_1$ transition show *no* resolved vibrational structure since the wave packet rapidly moves out of the Franck–Condon region to dissociation products. In contrast, the photodetachment transition from O_3^- to the O_3 $^1A_2$ state is fully allowed. In this case, the $t = 0$ wave packet will be the Franck–Condon projection of the anion ground state vibrational wave function onto the $^1A_2$ surface. By symmetry, the maximum amplitude of this wave packet will occur at $Q_3 = 0$ where the first derivative of the surface along the Q_3 coordinate is zero by definition. Recurrences along the bound normal coordinates, which are necessary for observing vibrational structure, are more likely to occur under these conditions. These considerations indicate that photodetachment should produce a more structured $^1A_2$ spectrum than absorption; the extent of the difference depends upon the actual steepness of the dissociation pathway in the vicinity of the barrier.

Given the complicated interactions between the O_3 excited states discussed above, it is perhaps surprising that the excited state region of the O_3^- photoelectron spectrum is as regular as it is. Clearly, this spectrum warrants a more detailed treatment than given here. For example, realistic simulations of the photoelectron spectrum should consider the effects of the multiple conical intersections in the O_3 excited state manifold. Strong vibronic coupling in the vicinity of these intersections[49] requires considerably more sophisticated simulation methods than the separable Franck–Condon model used in this paper. We hope that the data presented here stimulate further theoretical studies of this fundamentally important molecule.

V. CONCLUSIONS

We have presented photoelectron spectra of O_3^- obtained using photodetachment energies of 2.977, 4.657, and 5.822 eV. From the 2.977 eV spectrum, we determine a geometry for the ozonide anion ($r_e(O_3^-) = 1.36 \pm 0.02$ Å and $\theta_e(O_3^-) = 111.8 \pm 2°$). The 4.657 and 5.822 eV spectra show evidence of transitions to multiple electronic states. Laser polarization studies indicate that we are observing transitions to five excited states of O_3 below 3 eV in energy: The $^3A_2$, $^3B_2$, $^3B_1$, $^1A_2$, and $^1B_1$ states. Of importance to atmospheric chemists is the fact that we do not observe any evidence of electronic states lying below the ground state dissociation asymptote. Simulations of the data and comparison with published *ab initio* results indicate that the three lowest-lying electronic states have a $^1A_1$, $^3A_2$, $^3B_2$, energetic ordering, with the states lying at T_0 values of 0.0, 1.18, 1.30 eV, respectively. T_0 values of 1.45 and 1.58 eV are proposed for the $^3B_1$ and $^1A_2$ states, respectively; this assignment is more tentative, however. The large amount of vibrational structure above the dissociation limits of the excited states suggests that interesting dissociation dynamics occurs on these surfaces. The vibrational structure and polarization dependence of the data presented here serves as an excellent guide to determining the form and interaction of the low-lying electronic state potential energy surfaces, and it is hoped that these results will stimulate theoretical efforts along these lines.

ACKNOWLEDGMENTS

We would like to thank Professor S. M. Anderson for stimulating discussion and communication of *unpublished*

results. We thank Dr. M. Braunstein for communication of unpublished results and P. Ludowise for providing O_3. This work has been sponsored by the United States Air Force Office of Scientific Research under Contract No. AFOSR-91-0084.

[1] S. Solomon, Rev. Geophys. **26**, 131 (1988).
[2] R. Stolarski, R. Bojkov, L. Bishop, C. Zerefos, J. Staehelin, and J. Zawodny, Science **256**, 342 (1992).
[3] J. B. Kerr and C. T. McElroy, Science **262**, 1032 (1993).
[4] S. Solomon, Nature **347**, 347 (1990); D. J. Hofmann, S. J. Oltmans, J. M. Harris, S. Solomon, T. Deshler, and B. J. Johnson, *ibid.* **359**, 283 (1992).
[5] (a) P. J. Hay, T. H. Dunning, and W. A. Goddard III, Chem. Phys. Lett. **23**, 457 (1973); (b) D. Grimbert and A. Devaquet, Mol. Phys. **27**, 831 (1974); (c) P. J. Hay and T. H. Dunning, Jr., J. Chem. Phys. **67**, 2290 (1977); (d) K. H. Thunemann, S. D. Peyerimhoff, and R. J. Buenker, J. Mol. Spectrosc. **70**, 432 (1978); (e) R. O. Jones, J. Chem. Phys. **82**, 325 (1985); (f) A. Banichevich, S. D. Peyerimhoff, and F. Grein, Chem. Phys. Lett. **173**, 1 (1990); (g) M. Barysz, M. Rittby, and R. J. Bartlett, *ibid.* **193**, 373 (1992).
[6] (a) M. Braunstein, P. J. Hay, R. L. Martin, and R. T Pack, J. Chem. Phys. **95**, 8239 (1991); (b) M. Braunstein and R. T Pack, *ibid.* **96**, 6378 (1992).
[7] A. Banichevich and S. D. Peyerimhoff, Chem. Phys. **174**, 93 (1993).
[8] A. Banichevich, S. D. Peyerimhoff, J. A. Beswick, and O. Atabek, J. Chem. Phys. **96**, 6580 (1992).
[9] M. J. Chappuis, C. R. Acad. Sci. (Paris) **91**, 1985 (1980).
[10] O. R. Wulf, Proc. Natl. Acad. Sci. **16**, 507 (1930).
[11] P. J. Hay and W. A. Goddard III, Chem. Phys. Lett. **14**, 46 (1972).
[12] R. S. Mulliken, Can. J. Chem. **36**, 10 (1958).
[13] H. B. Levene, J.-C. Nieh, and J. J. Valentini, J. Chem. Phys. **87**, 2583 (1987).
[14] V. Vaida, D. J. Donaldson, S. J. Strickler, S. L. Stephens, and J. W. Birks, J. Phys. Chem. **93**, 506 (1989).
[15] A. D. Kirshenbaum and A. G. Streng, J. Chem. Phys. **35**, 1440 (1961).
[16] (a) S. M. Anderson, P. Hupalo, and K. Mauersberger, J. Chem. Phys. **99**, 737 (1993); (b) S. M. Anderson, J. Maeder, and K. Mauersberger, *ibid.* **94**, 6351 (1991); (c) S. M. Anderson, J. Morton, and K. Mauersberger, *ibid.* **93**, 3826 (1990).
[17] P. G. Burton and M. D. Harvey, Nature **266**, 826 (1977).
[18] C. L. Lin and M. T. Leu, Int. J. Chem. Kin. **14**, 417 (1982), and references therein.
[19] C. W. von Rosenberg, Jr. and D. W. Trainor, J. Chem. Phys. **61**, 2442 (1974).
[20] J. R. Locker, J. A. Joens, and E. J. Bair, J. Photochem. **36**, 235 (1987); T. Kleindienst, J. R. Locker, and E. J. Bair, *ibid.* **12**, 67 (1980).
[21] C. W. von Rosenberg, Jr., and D. W. Trainor, J. Chem. Phys. **63**, 5348 (1975).
[22] J. Shi and J. R. Barker, J. Phys. Chem. **94**, 8390 (1990).
[23] W. D. McGrath, J. M. Maguire, A. Thompson, and J. Trocha-Grimshaw, Chem. Phys. Lett. **102**, 59 (1983).
[24] N. Swanson and R. J. Celotta, Phys. Rev. Lett. **35**, 783 (1975).
[25] S. E. Novick, P. C. Engelking, P. L. Jones, J. H. Futrell, and W. C. Lineberger, J. Chem. Phys. **70**, 2652 (1979).
[26] *Advances in Gas Phase Chemistry*, Vol. 1, edited by N. G. Adams and L. M. Babcock (JAP, Greenwich, CT, 1992), pp. 121–166.
[27] K. M. Ervin, J. Ho, and W. C. Lineberger, J. Chem. Phys. **91**, 5974 (1989); D. G. Leopold, K. K. Murray, A. E. Stevens Miller, and W. C. Lineberger, J. Chem. Phys. **83**, 4849 (1985); H. B. Ellis, Jr., and G. B. Ellison, *ibid.* **78**, 6541 (1983).
[28] A. Weaver, D. W. Arnold, S. E. Bradforth, and D. M. Neumark, J. Chem. Phys. **94**, 1740 (1991); A. Weaver, R. B. Metz, S. E. Bradforth, and D. M. Neumark, J. Chem. Phys. **90**, 2070 (1989).
[29] R. B. Metz, A. Weaver, S. E. Bradforth, T. N. Kitsopoulos, and D. M. Neumark, J. Phys. Chem. **94**, 1377 (1990).
[30] D. Proch and T. Trickl, Rev. Sci. Instrum. **60**, 713 (1989).
[31] W. C. Wiley and I. H. McLaren, Rev. Sci. Instrum. **26**, 1150 (1955).
[32] J. Cooper and R. N. Zare, J. Chem. Phys. **48**, 942 (1968).
[33] K. M. Ervin, J. Ho, and W. C. Lineberger, J. Phys. Chem. **92**, 5405 (1988).
[34] H. S. W. Massey, *Negative Ions* (Cambridge University, Cambridge, 1976); K. Ervin, J. Ho, and W. C. Lineberger, J. Chem. Phys. **91**, 5974 (1991).
[35] T. Tanaka and Y. Morino, J. Mol. Spectrosc. **33**, 538 (1970); R. H. Hughes, J. Chem. Phys. **24**, 131 (1956); R. Trambarulo, S. N. Ghosh, C. A. Burrus, Jr., and W. Gordy, J. Chem. Phys. **21**, 538 (1953).
[36] E. B. Wilson, Jr., J. C. Decius, P. C. Cross, *Molecular Vibrations* (Dover, New York, 1980).
[37] P. Hennig and G. Strey, Z. Naturforsch. A **31**, 244 (1976).
[38] This value of $r_e(O_3^-)$ does not account for the difference between $r_e(O_3^-)$ and $r_0(O_3^-)$ resulting from anion vibrational anharmonicities which are presently undetermined. Likewise for the value of $\theta_e(O_3^-)$.
[39] L. J. Wang, S. B. Woo, and E. M. Helmy, Phys. Rev. A **35**, 759 (1987).
[40] R. C. Spiker, Jr. and L. Andrews, J. Chem. Phys. **59**, 1851 (1973); G. Steffen, W. Hesse, M. Jansen, and D. Reinen, Inorg. Chem. **30**, 1923 (1991).
[41] M. E. Jacox and D. E. Milligan, J. Mol. Spectrosc. **43**, 148 (1972); M. E. Jacox and D. E. Milligan, Chem. Phys. Lett. **14**, 518 (1972).
[42] M. R. Nimlos and G. B. Ellison, J. Phys. Chem. **90**, 2574 (1986).
[43] L. S. Cederbaum, W. Domcke, and W. von Niessen, Mol. Phys. **33**, 1399 (1977).
[44] S. M. Anderson and K. Mauersberger, J. Geophys. Res. (to be published).
[45] GAUSSIAN 92, Revision C, M. J. Frisch, G. W. Trucks, M. Head-Gordon, P. M. W. Gill, M. W. Wong, J. B. Foresman, B. G. Johnson, H. B. Schlegel, M. A. Robb, E. S. Replogle, R. Gomperts, J. L. Andres, K. Raghavachari, J. S. Binkley, C. Gonzalez, R. L. Martin, D. J. Fox, D. J. Defrees, J. Baker, J. J. P. Stewart, and J. A. Pople (Gaussian, Inc., Pittsburgh, PA, 1992).
[46] At the SCF-CISD/6-31G level of theory we obtain: $^3A_2 - r_{O-O}=1.365$ Å, $\theta=98.12°$, $\omega_1=1349$ cm^{-1}, $\omega_2=580$ cm^{-1}; $^3B_2 r_{O-O}=1.402$ Å, $\theta=108.56°$, $\omega_1=1380$ cm^{-1}, $\omega_2=579$ cm^{-1}.
[47] (a) R. Schinke and V. Engel, J. Chem. Phys. **93**, 3252 (1990); (b) K. C. Kulander and J. C. Light, *ibid.* **73**, 4337 (1980); (c) E. J. Heller, *ibid.* **68**, 3891 (1978); (d) R. T Pack, *ibid.* **65**, 4765 (1976).
[48] R. Schinke, *Photodissociation Dynamics* (Cambridge University, Cambridge, 1993), Chap. 8.
[49] H. Koppel, W. Domcke, and L. S. Cederbaum, Adv. Chem. Phys. **57**, 59 (1984).